The Lagrangian particle method for macroscopic and micro–macro viscoelastic flow computations[1]

P. Halin, G. Lielens, R. Keunings[*], V. Legat

CESAME, Division of Applied Mechanics, Université catholique de Louvain, B-1348 Louvain-la-Neuve, Belgium

Abstract

We propose a new numerical technique, referred to as the Lagrangian Particle Method (LPM), for computing time-dependent viscoelastic flows using either a differential constitutive equation (macroscopic approach) or a kinetic theory model (micro–macro approach). In LPM, the Eulerian finite element solution of the conservation equations is decoupled from the Lagrangian computation of the extra-stress at a number of discrete particles convected by the flow. In the macroscopic approach, the extra-stress carried by the particles is obtained by integrating the constitutive equation along the particle trajectories. In the micro–macro approach, the extra-stress is computed by solving along the particle paths the stochastic differential equation associated with the kinetic theory model. Results are given for the start-up flow between slightly eccentric rotating cylinders, using the FENE and FENE-P dumbbell models for dilute polymer solutions. © 1998 Elsevier Science B.V. All rights reserved.

Keywords: Finite element method; Stochastic simulation; FENE dumbbells

1. Introduction

To date, most numerical simulations of viscoelastic flows have been based on a purely *macroscopic* approach where one solves numerically the conservation laws together with a suitable rheological constitutive equation. Study of the monograph by Crochet, Davies and Walters [1] and of consecutive review papers (e.g. [2–5]) reveals that progress in macroscopic viscoelastic flow computations has been very impressive indeed. The subject, however, is by no means closed and further developments are still called for, such as improved techniques for time-dependent and three-dimensional flows. Since the pioneering work by Laso and Öttinger [6,7], a complementary *micro–macro* approach to viscoelastic flow simulations is now emerging that combines the solution of the conservation laws with the direct use of a kinetic theory model describing the fluid's rheology (e.g. [8–12]). In the micro–macro

---

* Corresponding author. Tel.: +32-10-47-23-50; fax: +32-10-47-21-80.
[1]Dedicated to Professor Marcel J. Crochet on the occasion of his 60th birthday.

approach, modeling is achieved at the coarse-grain level without resorting to closure approximations of questionable value, thus providing a direct link between the flow-induced development of the microstructure and the flow operating conditions.

In the present paper, we propose a new numerical technique, referred to as the Lagrangian Particle Method (LPM), for solving time-dependent viscoelastic flows with either the macroscopic or the micro–macro approach. LPM combines in a decoupled fashion the solution of the conservation laws with a Lagrangian computation of the extra-stress at a number of discrete particles that are convected by the flow. The extra-stress is computed by integrating along the particle paths either the relevant differential constitutive equation (macroscopic approach), or the stochastic differential equation associated to the kinetic theory model (micro–macro approach). For illustrative purposes, we consider the start-up flow of a dilute polymer solution between slightly eccentric rotating cylinders. The polymer solution is described by the kinetic theory of finitely extensible non-linear elastic (FENE) dumbbells. The FENE theory is used as such in the micro–macro LPM simulations, while its approximate macroscopic version, namely the FENE-P constitutive equation obtained with the Peterlin closure approximation [13], is used in the macroscopic LPM runs. In the micro-macro LPM simulations, each Lagrangian particle convected by the flow carries an ensemble of dumbbells. In LPM, these ensembles of dumbbells can be statistically uncorrelated or correlated. The latter case yields in fact a numerical approach that is equivalent, in the limit of vanishing discretization error, to the method of Brownian configuration fields introduced recently by Hulsen et al. [11].

The paper is organized as follows. In Section 2, we detail the relevant governing equations. Section 3 describes the basic technical features of LPM. The simulation results are reported in Section 4. Finally, we conclude in Section 5.

2. Governing equations

We consider the time-dependent isothermal flow of an incompressible viscoelastic fluid in a confined geometry. Expressed in Eulerian form, the conservation laws for linear momentum and mass read [14]

$$\rho \frac{\mathrm{D}\boldsymbol{v}}{\mathrm{D}t} = \nabla \cdot (-p\boldsymbol{I} + \boldsymbol{\tau}), \tag{1}$$

$$\nabla \cdot \boldsymbol{v} = 0, \tag{2}$$

where ρ is the density, p and $\boldsymbol{v}$ are the pressure and velocity fields, respectively, $\boldsymbol{I}$ is the unit tensor, $\boldsymbol{\tau}$ is the extra-stress tensor, and $(\mathrm{D}\boldsymbol{v}/\mathrm{D}t)$ is the material time derivative $(\partial \boldsymbol{v}/\partial t) + \boldsymbol{v} \cdot \nabla \boldsymbol{v}$. Note that we have neglected body forces in Eq. (1). For describing the rheology of polymer solutions, it is customary to define the extra-stress $\boldsymbol{\tau}$ as the sum of a viscous solvent contribution $\boldsymbol{\tau}_s$ and a polymer contribution $\boldsymbol{\tau}_p$,

$$\boldsymbol{\tau} = \boldsymbol{\tau}_s + \boldsymbol{\tau}_p, \quad \boldsymbol{\tau}_s = 2\eta_s \boldsymbol{D}, \tag{3}$$

where $\boldsymbol{D}$ is the rate of deformation tensor $\frac{1}{2}(\nabla \boldsymbol{v} + \nabla \boldsymbol{v}^{\mathrm{T}})$ and η_s is the constant shear viscosity of the solvent.

The conservation laws Eqs. (1) and (2) must be closed with a suitable model that relates the polymer stress $\boldsymbol{\tau}_p$ to the deformation of the fluid. In the present paper, we adopt for that purpose the kinetic theory of Warner finitely extensible non-linear elastic (FENE) dumbbells [13]. In this framework, the

polymer solution is viewed as a suspension of non-interacting dumbbells convected in a Newtonian solvent. A dumbbell is made of two identical Brownian beads connected by a spring. While the beads represent the interaction between the polymer and the solvent, the spring models intramolecular interactions. Carried by the macroscopic flow, the beads experience Brownian force, Stokes drag and the spring force. In this coarse grain picture, the configuration of the polymer is described by the length and orientation of the vector $\boldsymbol{Q}$ connecting the two beads. For FENE dumbbells, the spring force $\boldsymbol{F}^c$ is defined as

$$\boldsymbol{F}^c(\boldsymbol{Q}) = \frac{H}{1 - \boldsymbol{Q}^2/Q_0^2}\boldsymbol{Q}, \tag{4}$$

where H is a spring constant and Q_0 is the maximum spring length. Although quite simple, the kinetic theory of FENE dumbbells has been found recently to model many phenomena observed with dilute solutions (e.g. [15,16]). In particular, it is able to predict hysteretic behaviour in stress growth/relaxation experiments [17–19].

A central result of kinetic theory [13] is the diffusion equation that governs the evolution of the configuration distribution function $\psi(\boldsymbol{Q}, t)$, namely

$$\frac{\partial \psi}{\partial t} = -\frac{\partial}{\partial \boldsymbol{Q}} \cdot \left[\left\{\boldsymbol{\kappa} \cdot \boldsymbol{Q} - \frac{2}{\zeta}\boldsymbol{F}^c(\boldsymbol{Q})\right\}\psi\right] + \frac{2kT}{\zeta}\frac{\partial}{\partial \boldsymbol{Q}} \cdot \frac{\partial}{\partial \boldsymbol{Q}}\psi, \tag{5}$$

where ζ is the friction coefficient of the Brownian beads, T is the absolute temperature, k is the Boltzmann constant, and $\boldsymbol{\kappa}$ is the velocity gradient. The latter is assumed constant over the polymer (dumbbell) length scale. In non-homogeneous flows, the distribution function generally depends upon the spatial position $\boldsymbol{x}$, and the time derivative in Eq. (5) becomes in fact the material derivative $D\psi/Dt = \partial\psi/\partial t + \boldsymbol{v} \cdot \partial\psi/\partial\boldsymbol{x}$. A second key result of kinetic theory is an expression due to Kramers [13] that yields the polymer contribution to the stress:

$$\boldsymbol{\tau}_p = -nkT\boldsymbol{I} + n\langle\boldsymbol{Q}\boldsymbol{F}^c(\boldsymbol{Q})\rangle, \tag{6}$$

where n is the dumbbell number density and the angular brackets denote the configuration space average

$$\langle\cdot\rangle = \int \cdot\,\psi\,\mathrm{d}\boldsymbol{Q}. \tag{7}$$

For Hookean dumbbells (i.e. $Q_0 \to \infty$ in Eq. (4)), it is possible to derive from Eqs. (5) and (6) a closed-form constitutive equation for the polymer stress $\boldsymbol{\tau}_p$. This yields the Oldroyd-B model, with a relaxation time $\lambda = \zeta/4H$ and a polymer contribution to the shear viscosity $\eta_p = nkT\lambda$ [13]. When Q_0 has a finite value, however, it is impossible to obtain a macroscopic constitutive equation that is mathematically equivalent to the FENE kinetic model. In order to exploit Kramers' expression Eq. (6), one must either solve the diffusion Eq. (5), or, as done in the present work, integrate along the flow trajectories the associated Itô stochastic differential equation [20]:

$$\mathrm{d}\boldsymbol{Q} = \left[\boldsymbol{\kappa} \cdot \boldsymbol{Q} - \frac{2}{\zeta}\boldsymbol{F}^c(\boldsymbol{Q})\right]\mathrm{d}t + \sqrt{\frac{4kT}{\zeta}}\,\mathrm{d}\boldsymbol{W}. \tag{8}$$

Here, W is the three-dimensional Wiener process, namely a Gaussian stochastic process with vanishing mean and covariance $\langle W(t_1)W(t_2) \rangle = \min(t_1, t_2)I$. As discussed in [20], Eq. (8) is an evolution equation for the Markovian process Q whose probability density ψ is solution of the diffusion Eq. (5). In the stochastic simulation approach, the polymer stress τ_p is again obtained by means of Kramers' expression Eq. (6), with the configuration average Eq. (7) computed as an ensemble average over many realizations of the stochastic process Q.

In the present paper, we also propose a new approach to the numerical computation of viscoelastic flow problems with a differential constitutive equation. The FENE-P equation is used for illustrative purposes. It is based on a self-consistent pre-averaging approximation of the spring force Eq. (4) due to Peterlin,

$$F^c(Q) = \frac{H}{1 - \langle Q^2 \rangle / Q_0^2} Q. \tag{9}$$

The Peterlin closure approximation allows one to derive from the diffusion Eq. (5) the following evolution equation [13] for the configuration tensor $A = \langle QQ \rangle$:

$$\frac{\partial A}{\partial t} + v \cdot \nabla A - \kappa \cdot A - A \cdot \kappa^T = \frac{4kT}{\zeta}I - \frac{4H/\zeta}{1 - \mathrm{Tr}(A)/Q_0^2}A. \tag{10}$$

Use of Kramers' expression Eq. (6) and of the force law Eq. (9) then yields the FENE-P polymer stress in terms of the configuration tensor:

$$\tau_p = -nkTI + n\frac{H}{1 - \mathrm{Tr}(A)/Q_0^2}A. \tag{11}$$

As detailed in [13], Eqs. (10) and (11) lead to a non-linear differential constitutive equation for the polymer stress τ_p. In numerical work, it is more convenient to solve the configuration Eq. (10), and then compute the polymer stress using Kramers' expression Eq. (11).

The rheometrical responses of the FENE and FENE-P models are compared in [21,22], where it is shown that the Peterlin closure approximation can have a significant impact indeed. (For a markedly better closure approximation of the FENE theory, see [17].) The FENE and FENE-P models involve a time constant $\lambda = \zeta/4H$ and the dimensionless finite extensibility parameter $b = HQ_0^2/kT$. We also note for further reference that the polymer contribution to the zero shear rate viscosity is $\eta_p^0 = nkT\lambda b/(b + 3)$ for the FENE-P fluid, and $\eta_p^0 = nkT\lambda b/(b + 5)$ for the FENE theory.

3. The Lagrangian particle method

3.1. Basic features

The LPM is depicted schematically in Fig. 1. We decouple the Eulerian solution of the conservation Eqs. (1) and (2) from the Lagrangian computation of the polymer contribution to the stress. A typical time step goes as follows. Using the current polymer stress values, computed in each element (at the previous time step), a standard Galerkin finite element technique is applied to the conservation equations to yield the updated velocity and pressure fields. The new velocity field is then used to update
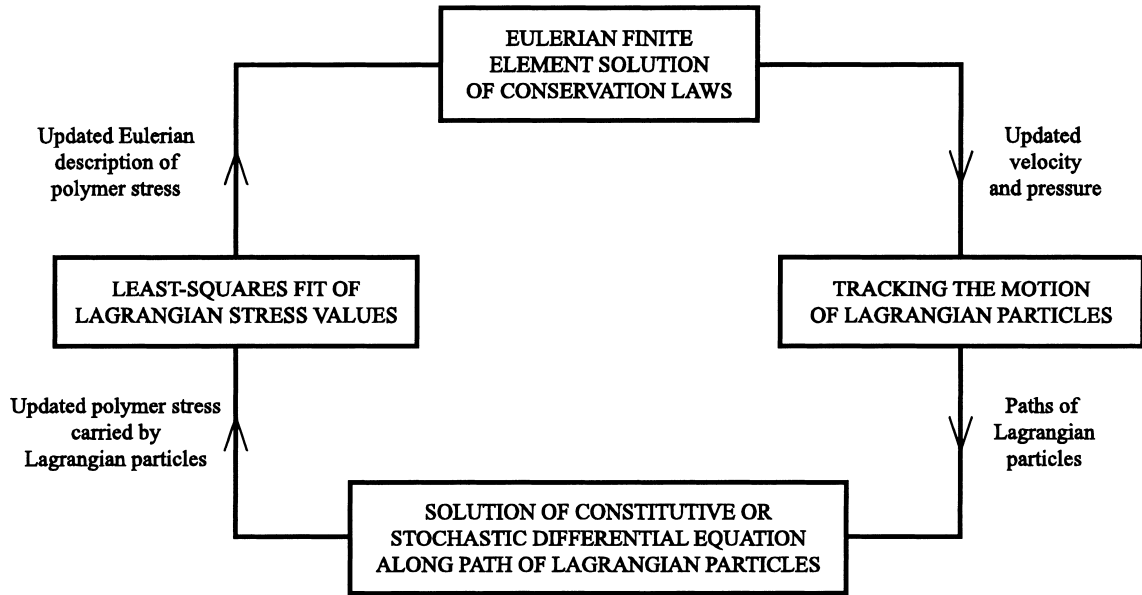
Fig. 1. Schematic of the Lagrangian particle method.

the polymer stress. In LPM, we compute the polymer stress at discrete Lagrangian particles which are convected by the flow. This is achieved by solving along the computed particle trajectories either the macroscopic constitutive Eqs. (10) and (11), or the stochastic differential Eq. (8) for a larger number of dumbbells carried by each particle. The polymer stress values thus obtained at the Lagrangian particles are converted into an Eulerian, element-by-element polynomial representation, which feeds the discretized conservation laws and allows for the calculation of the velocity and pressure fields at the next time step.

Let us now briefly review the main technical features of LPM.

3.2. Conservation equations

We consider time-dependent, two-dimensional (2D) flows in a domain Ω with a known boundary $\partial\Omega$. The flow domain is discretized by means of a *fixed* mesh of finite elements, over which the Eulerian velocity and pressure fields are approximated as

$$\boldsymbol{v}^a(\boldsymbol{x},t) = \sum_{i=1}^{N_v} \boldsymbol{v}^i(t)\psi_i(\boldsymbol{x}), \qquad p^a(\boldsymbol{x},t) = \sum_{j=1}^{N_p} p^j(t)\pi_j(\boldsymbol{x}). \tag{12}$$

Here ψ_i and π_j are given finite element basis functions, while $\boldsymbol{v}^i$ and p^j are unknown, time-dependent nodal values. The mesh being fixed, the shape functions depend on the spatial coordinates $\boldsymbol{x}$ only. We use Galerkin's principle (e.g. [3]) to discretize the conservation laws Eqs. (1) and (2). Residuals obtained after substitution of the approximations Eq. (12) in the governing Eqs. (1) and (2) are made orthogonal to the set of basis functions, and an integration by parts is performed in the discretized

momentum balance. The Galerkin equations read

$$\int_{\Omega} \psi_i \left[\rho \frac{D\boldsymbol{v}^{\mathrm{a}}}{Dt} \right] \mathrm{d}\Omega + \int_{\Omega} \nabla \psi_i^{T} \cdot \left[-p^{\mathrm{a}} \boldsymbol{I} + 2\eta_{\mathrm{s}} \boldsymbol{D}^{\mathrm{a}} + \boldsymbol{\tau}_{\mathrm{p}} \right] \mathrm{d}\Omega = \int_{\partial\Omega} \psi_i \boldsymbol{t} \, \mathrm{d}s, \tag{13}$$

$$\int_{\Omega} \pi_j [\nabla \cdot \boldsymbol{v}^{a}] \mathrm{d}\Omega = 0, \tag{14}$$

for $1 \leq i \leq N_\nu$ and $1 \leq j \leq N_p$. In Eqs. (13) and (14), every term with the superscript a denotes the corresponding finite element approximation obtained from the expansions Eq. (12), $\boldsymbol{t}$ is the contact force, and s the arc length measured along the boundary.

The Galerkin Eqs. (13) and (14) can be used to compute the velocity and pressure fields provided the polymer stress contribution to the discretized momentum balance Eq. (13), namely

$$\int_{\Omega} \nabla \psi_i^{\mathrm{T}} \cdot \boldsymbol{\tau}_p \, \mathrm{d}\Omega, \tag{15}$$

be known. In LPM, we treat Eq. (15) as a *known* pseudo-body force term. The Galerkin Eqs. (13) and (14) thus constitute a set of first-order differential equations for the nodal values of $\boldsymbol{v}^{\mathrm{a}}$ and p^{a}. In the current implementation of LPM, we discretize Eqs. (13) and (14) in time using the Euler forward/Euler backward predictor-corrector scheme with a constant time step Δt_{cons}. The solution of the implicit Euler backward equations is obtained by means of Newton's scheme, the initial guess being provided by the explicit Euler forward prediction. Finally, we use biquadratic continuous basis functions for the velocity, and bilinear continuous basis functions for pressure.

3.3. Tracking the motion of Lagrangian particles

In LPM, we compute the polymer stress $\boldsymbol{\tau}_{\mathrm{p}}$ at a number N_{part} of Lagrangian particles convected by the flow. Over a typical time step $[t_n, t_{n+1} = t_n + \Delta t_{\mathrm{cons}}]$, the trajectory of each Lagrangian particle is determined using the Eulerian velocity field obtained at time t_n. If $\boldsymbol{\tau}$ denotes the position vector of the particle, one thus solves the kinematic equation

$$\frac{\mathrm{d}\boldsymbol{r}}{\mathrm{d}t} = \boldsymbol{v}^{\mathrm{a}}(\boldsymbol{r}, t_n), \tag{16}$$

for t in $[t_n, t_{n+1}]$ and with the initial condition $\boldsymbol{r}(t_n)$ known from the previous time step. We integrate Eq. (16) by means of the tracking procedure proposed by Goublomme et al. [23] in the context of steady-state flows of integral viscoelastic fluids. The basic idea is to solve Eq. (16) in the parent finite element, using a fourth-order Runge–Kutta method. For this, we adopt a constant time step $\Delta t_{\mathrm{track}}$ such that $\Delta t_{\mathrm{track}} \leq \Delta t_{\mathrm{cons}}$. Knowledge of the particle trajectories between t_n and t_{n+1} allows us to compute the polymer stress $\boldsymbol{\tau}_{\mathrm{p}}$ at time t_{n+1}, as we now explain.

3.4. Differential constitutive equation

Most differential constitutive models currently used in computational rheology have the form

$$\frac{D\boldsymbol{\tau}_{\mathrm{p}}}{Dt} = \boldsymbol{f}(\boldsymbol{\tau}_{\mathrm{p}}, \boldsymbol{\kappa}). \tag{17}$$

With microstructural models such as the FENE-P equation, the evolution equation for the configuration tensor (see Eq. (10)) has a similar form:

$$\frac{DA}{Dt} = g(A, \kappa). \tag{18}$$

In LPM, we solve Eq. (17) or Eq. (18) along the flow trajectory of the N_{part} Lagrangian particles. The material derivative operator thus reduces to a simple time derivative taken along the pathlines. Over a typical time step $[t_n, t_{n+1} = t_n + \Delta t_{\text{cons}}]$, we use the Eulerian velocity field obtained at time t_n to integrate Eq. (17) or Eq. (18). With the FENE-P model, one thus solves for each particle

$$\frac{DA(r(t))}{Dt} = g(A(r(t)), \kappa^a(r(t), t_n)), \tag{19}$$

along the trajectory $\{r(t), t \in [t_n, t_{n+1}]\}$ and with the initial condition $A(r(t_n))$ known from the previous time step. For this, we use a fourth-order Runge–Kutta method with a constant time step Δt_{const} such that $\Delta t_{\text{track}} \leq \Delta t_{\text{const}} \leq \Delta t_{\text{cons}}$. Having obtained $A(r(t_{n+1}))$, we compute the updated polymer stress $\tau_p(r(t_{n+1}))$ by means of Kramers' expression (11).

3.5. Kinetic theory model

Computation of the polymer stress with the kinetic dumbbell model is achieved by solving the stochastic differential Eq. (8) along the trajectory of the N_{part} Lagrangian particles. For simplicity, we write all subsequent equations in dimensionless form. The connector vector Q, the time t, the velocity gradient and the polymer stress τ_p are made dimensionless with $(kT/H)^{1/2}, \lambda, \lambda^{-1}$, and nkT, respectively, and we define the notation $h(x) = 1/(1 - x/b)$. For FENE dumbbells, the dimensionless connector force reads

$$F^c(Q) = h(Q^2)Q, \tag{20}$$

while for FENE-P dumbbells we have

$$F^c(Q) = h(\langle Q^2 \rangle)Q. \tag{21}$$

Finally, the dimensionless Kramers' expression Eq. (6) is

$$\tau_p = \langle QF^c \rangle - I. \tag{22}$$

Each Lagrangian particle carries a number N_d of dumbbells. Over the time step $[t_n, t_{n+1} = t_n + \Delta t_{\text{cons}}]$, the configuration Q of each dumbbell is obtained by solving Eq. (8) using the Eulerian velocity field at time t_n,

$$dQ(r(t)) = [\kappa^a(r(t), t_n) \cdot Q(r(t)) - \tfrac{1}{2}F^c(Q(r(t)))] \, dt + dW, \tag{23}$$

along the trajectory $\{r(t), t \in [t_n, t_{n+1}]\}$ and with the initial condition $Q(r(t_n))$ known from the previous time step. In view of Kramers' expression Eq. (22), the updated polymer stress carried by a particle is then approximated by the ensemble average

$$\tau_{\mathrm{p}}(\boldsymbol{r}(t_{n+1})) = \frac{1}{N_{\mathrm{d}}} \sum_{i=1}^{N_{\mathrm{d}}} \boldsymbol{Q}^{(i)}(\boldsymbol{r}(t_{n+1})) \boldsymbol{F}^c(\boldsymbol{Q}^{(i)}(\boldsymbol{r}(t_{n+1}))) - \boldsymbol{I}, \tag{24}$$

where $\boldsymbol{Q}^{(i)}$ is an individual realization of the stochastic process $\boldsymbol{Q}$, and $\boldsymbol{F}^c$ is evaluated using either the FENE Eq. (20) or FENE-P Eq. (21) spring law.

For FENE-P dumbbells, we integrate Eq. (23) by means of the explicit Euler–Maruyama scheme, using a constant time step $\Delta t_{\mathrm{stoch}}$ such that $\Delta t_{\mathrm{track}} \leq \Delta t_{\mathrm{stoch}} \leq \Delta t_{\mathrm{cons}}$. This yields the simple recurrence

$$\boldsymbol{Q}(\boldsymbol{r}(t_{j+1})) = \boldsymbol{Q}(\boldsymbol{r}(t_j)) + [\boldsymbol{\kappa}^{\mathrm{a}}(\boldsymbol{r}(t_j), t_n) \cdot \boldsymbol{Q}(\boldsymbol{r}(t_j)) - \tfrac{1}{2} \boldsymbol{F}^c(\boldsymbol{Q}(\boldsymbol{r}(t_j)))] \Delta t_{\mathrm{stoch}} + \Delta \boldsymbol{W}_j, \tag{25}$$

for $t_{j+1} = t_j + \Delta t_{\mathrm{stoch}}$ in the interval $[t_n, t_{n+1}]$. The vector of Wiener increments $\Delta \boldsymbol{W}_j$ has independent Gaussian components with zero mean and variance $\Delta t_{\mathrm{stoch}}$.

The Euler–Maruyama scheme Eq. (25) is of weak order 1 [20]. When used with FENE dumbbells, it can lead to difficulties if $\Delta t_{\mathrm{stoch}}$ is too large. Indeed, an individual dumbbell can have its dimensionless length become larger than the upper bound $\sqrt{b}$, which is unphysical. Thus, for FENE dumbbells, we solve Eq. (23) by means of the semi-implicit predictor–corrector scheme proposed by Öttinger [20]. The predictor is the Euler scheme (25), which gives $\tilde{\boldsymbol{Q}}(\boldsymbol{r}(t_{j+1}))$. The corrector has the form

$$[1 + \tfrac{1}{4} h(\boldsymbol{Q}^2(\boldsymbol{r}(t_{j+1}))) \Delta t_{\mathrm{stoch}}] \boldsymbol{Q}(\boldsymbol{r}(t_{j+1})) = \boldsymbol{d}(\boldsymbol{Q}(\boldsymbol{r}(t_j)), \tilde{\boldsymbol{Q}}(\boldsymbol{r}(t_{j+1})), \Delta \boldsymbol{W}_j), \tag{26}$$

where the known vector $\boldsymbol{d}$ is given by

$$\begin{aligned} \boldsymbol{d} = \boldsymbol{Q}(\boldsymbol{r}(t_j)) &+ \tfrac{1}{2} [\boldsymbol{\kappa}^{\mathrm{a}}(\boldsymbol{r}(t_{j+1}), t_n) \cdot \tilde{\boldsymbol{Q}}(\boldsymbol{r}(t_{j+1})) + \boldsymbol{\kappa}^{\mathrm{a}}(\boldsymbol{r}(t_j), t_n) \cdot \boldsymbol{Q}(\boldsymbol{r}(t_j)) \\ &- \tfrac{1}{2} h(\boldsymbol{Q}^2(\boldsymbol{r}(t_j))) \boldsymbol{Q}(\boldsymbol{r}(t_j))] \Delta t_{\mathrm{stoch}} + \Delta \boldsymbol{W}_j. \end{aligned} \tag{27}$$

The update $\boldsymbol{Q}(\boldsymbol{r}(t_{j+1}))$ is a vector with direction $\boldsymbol{d}$ and length q that is solution of a cubic algebraic equation derived from Eq. (26). As shown in [20], q is unique and always in $[0, \sqrt{b}[$. The predictor–corrector scheme Eqs. (26) and (27) is of weak order 2.

In Eqs. (25)–(27), the Gaussian increments $\Delta \boldsymbol{W}_j$ can be replaced by other random variables that are cheaper to generate. As in [22], we use uniformly distributed random numbers whose moments are selected such as to keep unchanged the weak order of the numerical schemes [20].

An important issue to consider is that of the statistical correlation between ensembles of dumbbells carried by neighboring Lagrangian Particles [24]. The standard approach [7] uses uncorrelated ensembles in the sense that $N_{\mathrm{part}} \times N_{\mathrm{d}}$ independent Wiener processes govern the stochastic evolution of the dumbbells. Alternatively, if the same initial ensemble of dumbbells is used in each Lagrangian particles, and if the same N_{d} independent Wiener processes are generated to compute the configuration of corresponding dumbbells in each particle, then strong correlations develop in the polymer stress fluctuations at neighboring particles, which have almost identical flow histories. As discussed in [24], variance reduction should result from the cancellation of these fluctuations when taking the divergence of the polymer stress in the momentum balance Eq. (1). Use of correlated ensembles of dumbbells is the basic idea behind the method of Brownian configuration fields introduced by Hulsen et al. [11]. As discussed in [11,24], it dramatically reduces the spatial fluctuations of the computed velocity and stress fields, while decreasing the cost of generating the random numbers. In fact, LPM with correlated ensembles of dumbbells can de viewed as a Lagrangian particle solution of Eq. (11) in [11] that governs

a particular configuration field. Their number N_{f} of configuration fields thus corresponds to our number N_{d} of dumbbells carried by each lagrangian particle.

3.6. Computation of the polymer stress integral

At the end of a typical time step for the solution of the conservation laws, say at time t_{n+1}, we thus, have at our disposal values of the polymer stress $\boldsymbol{\tau}_{\mathrm{p}}$ at discrete Lagrangian Particle located at $\boldsymbol{r}^l(t_{n+1})$, for $l = 1, 2, \ldots, N_{\mathrm{part}}$. The last computational task to discuss is that using out these Lagrangian results to feed the Eulerian discretized momentum balance Eq. (13). In other words, one must compute the polymer stress integral Eq. (15) that will be used in the momentum balance Eq. (13) to update the velocity field at time $t_{n+2} = t_{n+1} + \Delta t_{\mathrm{cons}}$.

To do so, we compute in each finite element the linear least-squares polynomial that best fits the available polymer stress data, on the basis of the Lagrangian particles that are found present in the element at time t_{n+1}. The resulting piecewise-continuous Eulerian representation of $\boldsymbol{\tau}_{\mathrm{p}}$ is then used to evaluate the integrand of Eq. (15) at all integration points of the finite element mesh. Clearly, this procedure requires that at least three Lagrangian particles be present in each element at all discrete times when the polymer stress integral is evaluated.

4. Results for start-up flow in a journal bearing

4.1. Problem description

We consider the time-dependent, planar flow of FENE and FENE-P fluids between slightly eccentric cylinders, starting from the rest state (Fig. 2). The inner cylinder, of radius R_{i}, is rotating at a constant angular velocity ω, while the outer cylinder, of radius R_{o}, is fixed. The axes of the two cylinders are separated by a small eccentricity e. We assume that the fluid sticks to the cylinder walls, and specify the rest state as initial conditions. Thus, $\boldsymbol{v}^{\mathrm{a}}(\boldsymbol{x}, t = 0)$ is set to $\boldsymbol{0}$ over Ω. When using the macroscopic FENE-P constitutive equation, the initial configuration tensor $\boldsymbol{A}$ is set to its equilibrium value identically (this amounts to specifying $\boldsymbol{\tau}_{\mathrm{p}}(\boldsymbol{x}, t = 0) = \boldsymbol{0}$ over Ω. In the stochastic simulations, the initial dumbbell configurations in each Lagrangian particle are generated using the equilibrium distribution function [13].

The particular flow parameters and material data used in this work are listed in Table 1. The present flow problem is characterized by the dimensionless eccentricity $\epsilon = e/(R_{\mathrm{o}} - R_{\mathrm{i}}) = 0.1$, the dimensionless thickness $\mu = (R_{\mathrm{o}} - R_{\mathrm{i}})/R_{\mathrm{i}} = 0.1$, the Reynolds number $\mathrm{Re} = \rho \omega R_{\mathrm{i}}(R_{\mathrm{o}} - R_{\mathrm{i}})/(\eta_{\mathrm{s}} + \eta_{\mathrm{p}}^0) = 1.1$, the Deborah number $\mathrm{De} = \lambda \omega R_{\mathrm{i}}/(R_{\mathrm{o}} - R_{\mathrm{i}}) = 3$, the dimensionless finite extensibility $b=50$, and the viscosity ratio $\beta = \eta_{\mathrm{s}}/(\eta_{\mathrm{s}} + \eta_{\mathrm{p}}^0) = 1/9$.

Table 1
Flow parameters and material data used in the simulations (expressed in an arbitrary consistent system of units)

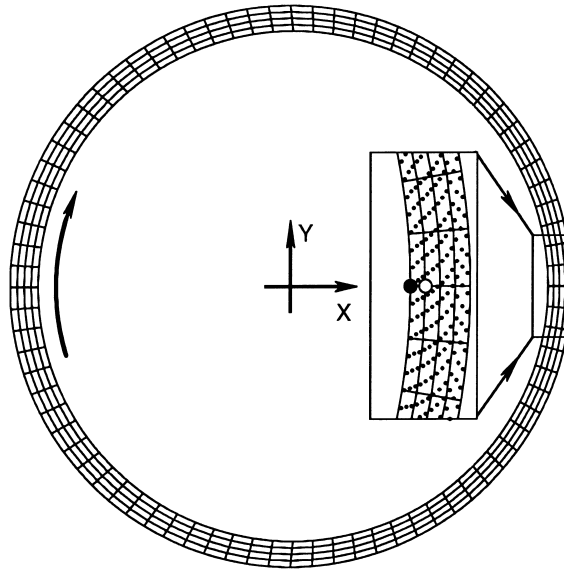| Flow parameters	$R_{\mathrm{i}}=10$	$R_{\mathrm{o}}=11$	$e=0.1$	$\omega=0.1$	
Material data	$\lambda=3$	$b=50$	$\rho=0.1$	$\eta_s=0.1$	$\eta_p^0=0.8$

Fig. 2. Finite element mesh for computing the start-up flow in a journal bearing. The enlargement shows a number of Lagrangian particles convected by the flow, as well as the locations where the computed polymer stress ($\bullet$) and velocity ($\bigcirc$) are displayed in subsequent figures.

A typical finite element mesh is shown in Fig. 2. We use structured grids with $N_r \times N_\theta$ quadrilateral elements, where N_r and N_θ are the number of uniformly-distributed elements in the radial and azimuthal directions respectively. Most numerical results shown in this section have been obtained with the 4×80 mesh of Fig. 2. For validation purposes, computations have also been performed with 8×80 and 4×160 meshes, with identical results at the scale of the figures shown here [25]. The numerical solutions will be presented in terms of the temporal evolution of the velocity and polymer stress in the region of narrowest gap (Fig. 2).

4.2. Macroscopic LPM computations with the FENE-P model

The results obtained with LPM applied to the FENE-P constitutive model Eqs. (10) and (11) are shown in Fig. 3. Contrary to the Newtonian solution (Re=1.1, De=0), the FENE-P velocity component ν_y reaches its steady value in an oscillatory fashion. A similar behaviour is predicted for the components of the polymer stress. These LPM results have been obtained with a total of $N_{\text{part}} = 2880$ Lagrangian particles that were uniformly distributed (i.e. 9 per element) at time $t=0$. The time steps were set to $\Delta t_{\text{cons}} = 10^{-2}$ and $\Delta t_{\text{track}} = \Delta t_{\text{const}} = 10^{-3}$.

In order to validate the LPM results, we have also computed the FENE-P solution using the mixed finite element method implemented by Purnode and Crochet [26]. In this method, the Galerkin principle is applied to both the conservation and constitutive equations. Quadrilateral elements are used with linear, quadratic and 4×4 linear sub-elements for the pressure, the velocity and the configuration tensor, respectively. The time stepping scheme is the Euler predictor-corrector method. Fig. 3 shows the results obtained with the mixed method, using the mesh of Fig. 2 and a time step $\Delta t = 10^{-2}$. The agreement with the results provided by LPM is excellent.
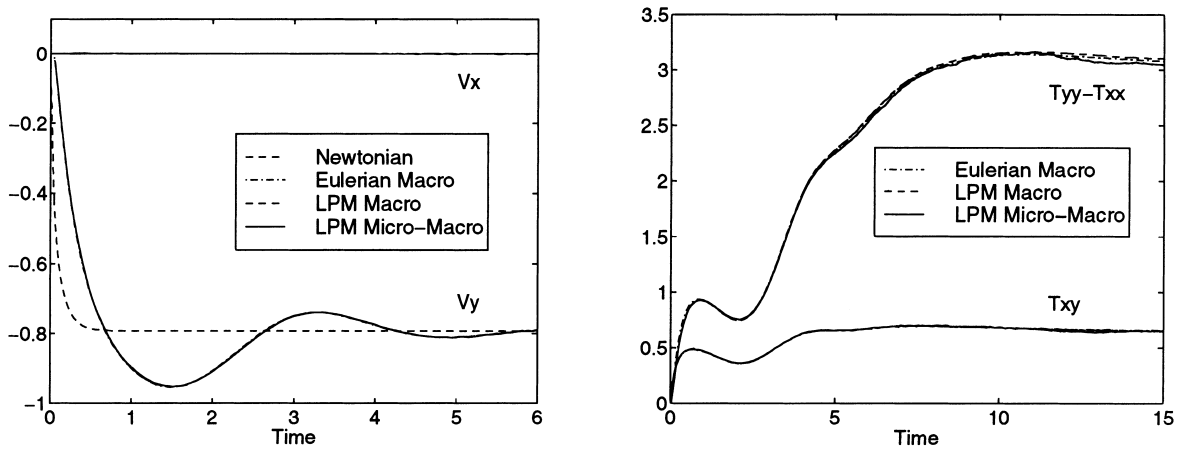
Fig. 3. Temporal evolution of velocity and polymer stress in the region of thinnest gap (see Fig. 2) obtained with the FENE-P constitutive equation. The Newtonian velocity is shown for reference. Results of the macroscopic and micro–macro LPM simulations are in excellent agreement with those obtained by means of the mixed finite element method (Eulerian macro).

4.3. Micro–macro LPM computations with FENE-P dumbbells

Before discussing results for the FENE kinetic theory, it is useful to evaluate the stochastic LPM approach with FENE-P dumbbells. We plot in Fig. 3 the FENE-P results defined as the mean of three independent micro–macro LPM simulations, using $N_d = 4500$ dumbbells in each of the $N_{part} = 2880$ Lagrangian particles. In these simulations, we used correlated ensembles of dumbbells. The time steps were set to $\Delta t_{cons} = 10^{-2}$ and $\Delta t_{track} = \Delta t_{stoch} = 10^{-3}$. Agreement between the macroscopic and micro–macro results is excellent. In comparison with the results obtained for the same problem by means of the first-generation CONNFFESSIT code of Laso and Öttinger (see Figs. 1 and 2 in Halin et al. [27]), the micro–macro LPM results are almost devoid of stochastic noise, especially in the velocity field. This is confirmed by inspection of Fig. 4 where we show the results of three individual micro-macro LPM runs, obtained with correlated or uncorrelated ensembles of dumbbells. With the rather large number of dumbbells for each Lagrangian particle, the fluctuations are only slightly reduced using correlated ensembles.

The effect of variance reduction brought about by the use of correlated ensembles of dumbbells is much more dramatic in Fig. 5. Here, present the results of nine independent LPM simulations using only $N_d = 450$ dumbbells in each Lagrangian particle. The fluctuations in the stress and velocity are much reduced with correlated ensembles of dumbbells. One should note, however, that the polymer stress results obtained with correlated ensembles, though much smoother, do vary a lot from one run to the other. In addition, the average over the nine independent runs is less accurate than that computed with uncorrelated ensembles. A plausible explanation is that, with such a small number of dumbbells in each particle, the use of correlated ensembles does not allow for an accurate generation of the initial equilibrium distribution.

Stochastic micro–macro simulations are mainly limited by the availability of computer memory. Using a fixed set of numerical parameters, including N_{part} and N_d, it may be practically feasible to average the results of a number *NR* of independent LPM realizations, while a single run with *NR* times
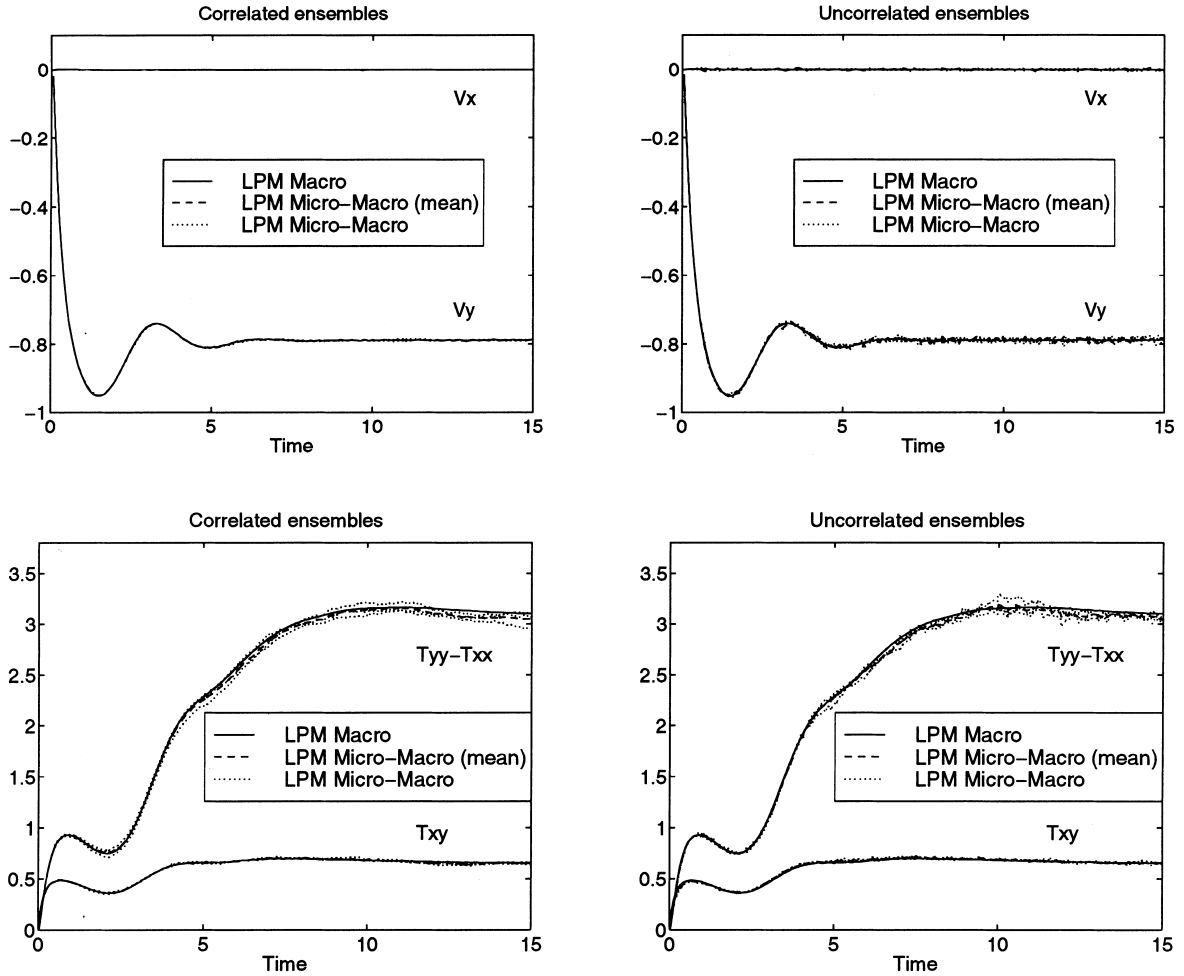
Fig. 4. Temporal evolution of velocity and polymer stress in the region of thinnest gap (see Fig. 2) obtained with the FENE-P constitutive equation. Three individual micro–macro LPM simulation results, obtained with correlated or uncorrelated ensembles of 4500 dumbbells in each Lagrangian particle, are compared to their macroscopic LPM counterparts. The average of the three individual micro-macro results is also shown.

more dumbbells in each particle would not fit the available memory. In view of the non-linear coupling between polymer stress and velocity, it is not obvious that this simple averaging procedure behaves satisfactorily. Fig. 6 provides a positive answer in that regard, at least for the flow problem considered here.

Let $R^{(i)}(t)$ denote the result of the ith stochastic LPM run at time t. We take the corresponding macroscopic LPM result $R_{\mathrm{macro}}(t)$ as a reference solution. Using a number nr of independent results ($1 \le nr \le NR$), one obtains the average

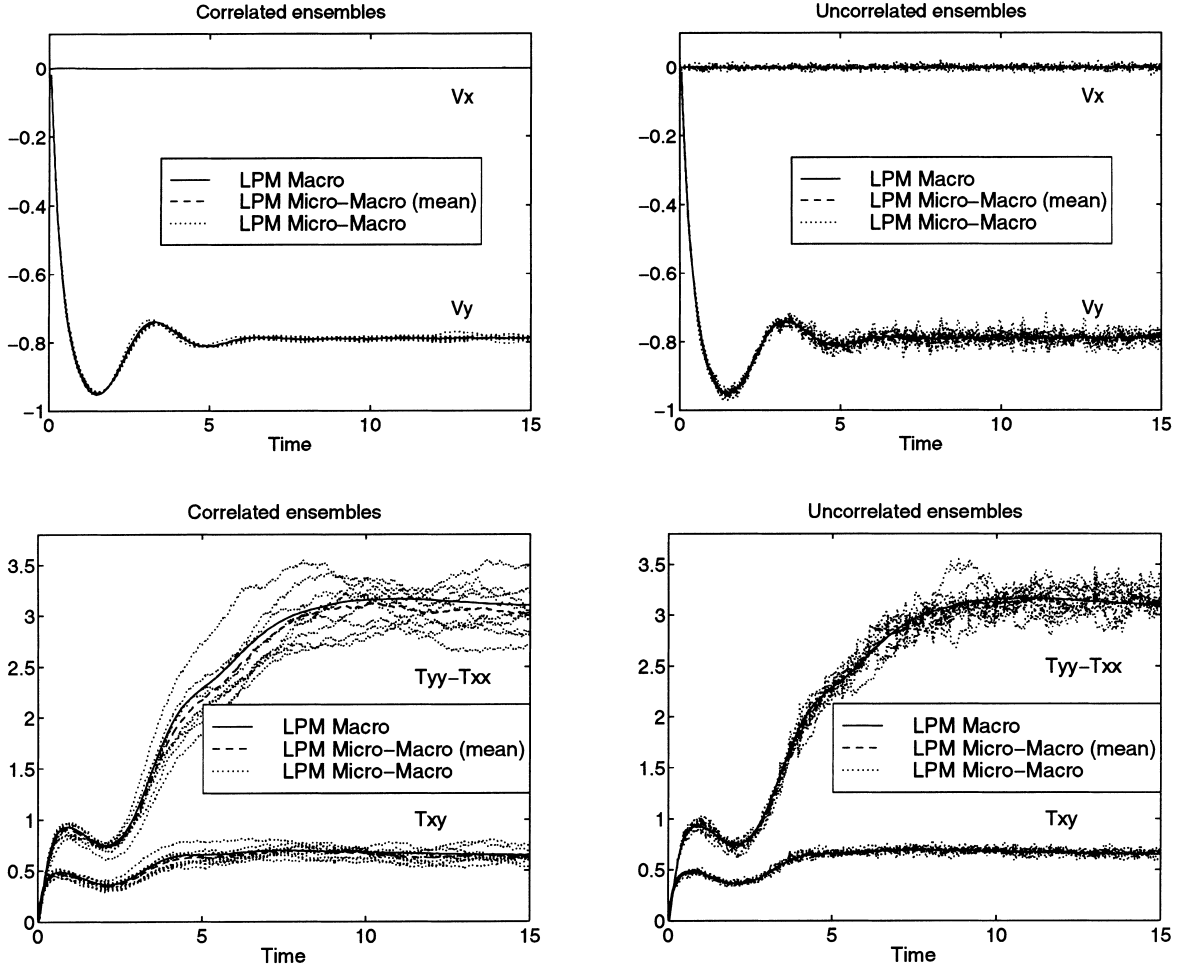$$R_{av}^{(\mathrm{nr})}(t) = \frac{1}{nr} \sum_{i=1}^{nr} R^{(i)}(t). \tag{28}$$

Fig. 5. Temporal evolution of velocity and polymer stress in the region of thinnest gap (see Fig. 2) obtained with the FENE-P constitutive equation. Nine individual micro–macro LPM simulation results, obtained with correlated or uncorrelated ensembles of 450 dumbbells in each Lagrangian particle, are compared to their macroscopic LPM counterparts. The average of the nine individual micro–macro results is also shown.

An estimate of the numerical error carried by this average is given by the mean quadratic error

$$e^{(\mathrm{nr})} = \frac{1}{t_{\mathrm{f}} - t_0} \int_{t_0}^{t_{\mathrm{f}}} [R_{\mathrm{av}}^{(\mathrm{nr})}(t) - R_{\mathrm{macro}}(t)]^2 \mathrm{d}t, \qquad (29)$$

where the relevant time interval $[t_0, t_{\mathrm{f}}]$ is set to [0, 15] in the present case (cfr. Fig. 4). Since we have a total of NR independent LPM results at our disposal, there are $N(\mathrm{nr}) = NR!/nr!(NR - nr)!$ ways of forming the average Eq. (28), each carrying a mean quadratic error Eq. (29). It is the average of these errors, computed over the $N(\mathrm{nr})$ possible combinations, that is plotted in Fig. 6 as a function of nr. Here, the result R being considered is either the velocity or the polymer stress. The evolution of the average
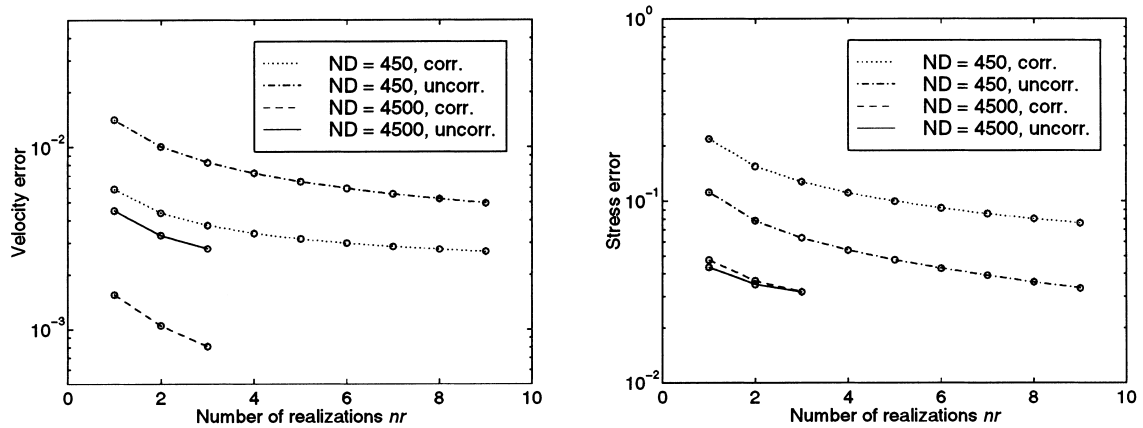
Fig. 6. Average error for the micro–macro LPM velocity and normal stress difference as a function of the number *nr* of independent LPM realizations (FENE-P model).

error is indeed consistent with the $1/\sqrt{nr}$ behavior that would be obtained without the stress–velocity coupling.

4.4. Micro–macro LPM computations with FENE dumbbells

Finally, we show in Fig. 7 the stochastic LPM results obtained with FENE dumbbells. As in Fig. 3, we plot the average results computed over three independent LPM runs, with $N_d = 4500$, $N_{part} = 2880$ and correlated ensembles of dumbbells. The time steps are as in Section 4.3. Inspection of Fig. 7 reveals the significant impact of the Peterlin approximation, already observed in simple rheometrical flows [21,22].
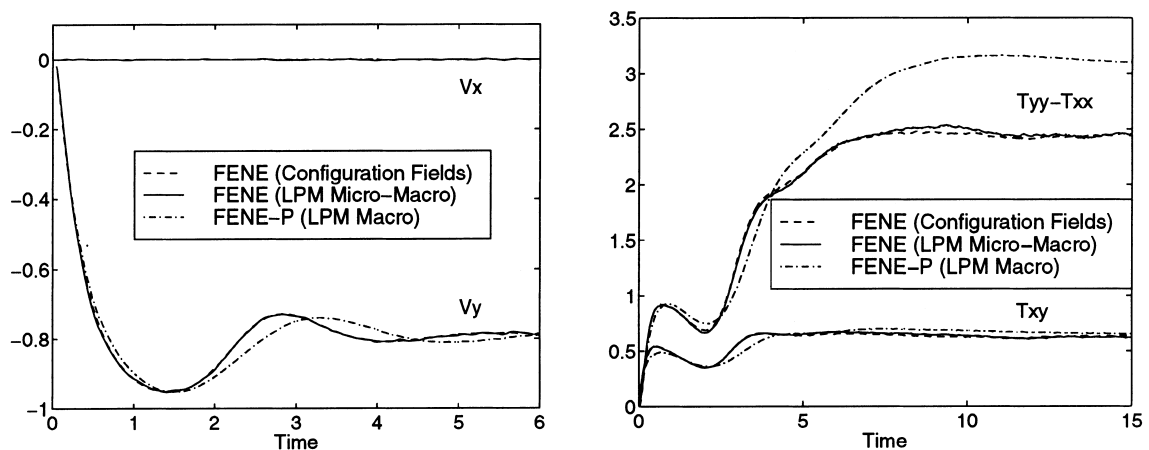

Fig. 7. Temporal evolution of velocity and polymer stress in the region of thinnest gap (see Fig. 2) obtained with the FENE kinetic theory and the FENE-P constitutive equation. Also shown are the FENE results obtained in [28] by means of the method of Brownian configuration fields.

We also show in Fig. 7 the results obtained by our T.U. Delft colleagues [28] for the same flow problem, using their Brownian configuration fields approach [11]. The agreement with the LPM results is very good indeed.

5. Discussion and conclusions

The above results demonstrate the ability of LPM to produce accurate numerical results in a non-trivial time-dependent viscoelastic flow problem, using either a macroscopic constitutive equation of the differential type or a kinetic theory model for the polymer dynamics.

Table 2 summarizes the computer resources (CPU time and main memory capacity) needed for obtaining the results illustrated in Figs. 3–5 for FENE-P dumbbells with the 4×80 finite element mesh. The particular computer used in this work is a SGI Indigo2 R10000 workstation.

We wish to point out that the data in Table 2 for the Eulerian macroscopic simulation are only shown for the sake of completeness, and are not representative of the state-of-the-art of Eulerian methods for transient viscoelastic flows. Indeed, the implicit mixed method implemented by Purnode and Crochet [26] was not designed with transient flows in mind as it solves at each time step the full set of discretized equations by means of a Newton scheme, which of course is rather expensive. At any rate, the macroscopic LPM approach is quite attractive in terms of computer resources. Another strong point of the new technique is the stability and accuracy of the Lagrangian integration of the constitutive equation along the particle paths. Indeed, LPM takes account in a most natural way of the purely convective nature of differential viscoelastic constitutive equations.

The micro–macro LPM runs, with either correlated or uncorrelated ensembles of dumbbells, are significantly more expensive than macroscopic computations, but they remain feasible on available hardware. This is of course the price to pay for the direct use in flow simulation of kinetic theory models, such as the FENE dumbbell model, which cannot be translated into an equivalent macroscopic constitutive equation. Use of correlated ensembles of dumbbells not only reduces the statistical noise affecting the results but also does decrease the CPU time by almost a factor of two in the present case. One should also note that tracking the motion of the Lagrangian particles and the expensive task of evaluating the particle polymer stress can be implemented on parallel computers using algorithms similar to those already developed for integral constitutive equations [29–31].

A number of numerical issues related to LPM still deserves further investigation. In particular, theoretical developments are needed to better understand the transfer of information between the Lagrangian stress calculation and the Eulerian conservation equations, and the smoothing effect that this transfer may have. In this work, we used successfully a piecewise discontinuous least-squares

Table 2
Computer resources for the FENE-P simulations of Figs. 3–5, with $\Delta t_{\text{cons}} = 10^{-2}$ and $[t_0, t_f] = [0,15]$

Method	N_{part}	N_{d}	CPU (s)	Memory (MB)
Eulerian macro	–	–	62 285	81
LPM macro	2880	–	2 607	16
LPM micro–macro (correlated ensembles)	2880	4500	94 900	313
LPM micro–macro (uncorrelated ensembles)	2880	4500	165 791	313

interpolation of the Lagrangian polymer stress values. Use of continous least-squares interpolation produced numerical instabilities [25] for reasons which remain to be understood. The numerical implications of using correlated ensembles of dumbbells with LPM also deserve further study. As demonstrated in the present work, LPM can also be used with uncorrelated ensembles of dumbbells for problems where the physical fluctuations become relevant [24]. Finally, criteria remain to be developed for selecting optimal values of the numerical parameters (number of Lagrangian particles, number of dumbbells, and the various time steps) for a given flow problem and its spatial discretization.

The major next step in the development of LPM is the design of an *adaptive* algorithm that would allow the automatic creation or deletion of Lagrangian particles when and where needed, in order to meet specific accuracy requirements. Other useful extensions of LPM include the use of integral constitutive equations and their related stochastic formulations [32,33], the implementation of capabilities for free-surface flows, and porting to parallel computer. We plan to report on these developments in the near future.

Acknowledgements

References

[1] M.J. Crochet, A.R. Davies, K. Walters, Numerical Simulation of Non-Newtonian Flow, Elsevier, Amsterdam, 1984.

[2] M.J. Crochet, Simulation of viscoelastic flow. Rubber Chemistry and Technology, Am. Chem. Soc. 62 (1989) 426–455.

[3] R. Keunings, Simulation of viscoelastic fluid flow, in: C.L. Tucker III, (Ed.), Fundamentals of Computer Modeling for Polymer Processing, Hanser, Munich, 1989, pp. 402–470.

[4] R. Keunings, P. Halin, Macroscopic and mesoscale approaches to the computer simulation of viscoelastic flows in: J.R.A. Pearson, M.J. Adams, R.A. Mashelkar, A.R. Rennie (Eds.), Dynamics of Complex fluids, Imperial College Press, The Royal Society, 1998, in press.

[5] F.P.T. Baaijens, Mixed finite element methods for viscoelastic flow analysis: a review, J. Non-Newtonian Fluid Mech., 1998, this volume.

[6] H.C. Öttinger, M. Laso, 'Smart' polymers in finite-element calculations, in: P. Moldenaers, R. Keunings, (Eds.), Proc. 10th Int. Congr. on Rheology, Elsevier, Amsterdam, 1992, pp. 286–288.

[7] M. Laso, H.C. Öttinger, Calculation of viscoelastic flow using molecular models: the CONNFFESSIT approach, J. Non-Newtonian Fluid Mech. 47 (1993) 1–20.

[8] K. Feigl, M. Laso, H.C. Öttinger, The CONNFFESSIT approach for solving a two-dimensional viscoelastic fluid problem, Macromolecules 28 (1995) 3261–3274.

[9] C.C. Hua, J.D. Schieber, Application of kinetic theory models in spatiotemporal flows for polymer solutions, liquid crystals and polymer melts using the CONNFFESSIT approach, Chem. Eng. Sci. 51 (1996) 1473–1485.

[10] M. Laso, M. Picasso, H.C. Öttinger, 2D time-dependent viscoelastic flow calculations using CONNFFESSIT, AIChE J. 43 (1997) 877–892.

[11] M.A. Hulsen, A.P.G. van Heel, B.H.A.A. van den Brule, Simulation of vicoelastic flows using Brownian configuration fields, J. Non-Newtonian Fluid Mech. 70 (1997) 79–101.

[12] T.W. Bell, G.H. Nyland, J.J. de Pablo, M.D. Graham, Combined Brownian dynamics and spectral simulation of the recovery of polymeric fluids after shear flow, Macromolecules 30 (1997) 1806–1812.

[13] R.B. Bird, C.F. Curtiss, R.C. Armstrong, O. Hassager, Dynamics of Polymeric Liquids, Kinetic theory, 2nd ed., vol. 2, Wiley-Interscience, New York, 1987.

[14] R.B. Bird, R.C. Armstrong, O. Hassager, Dynamics of Polymeric Liquids, Fluid mechanics, 2nd ed., vol. 1, Wiley-Interscience, New York, 1987.

[15] R.G. Larson, T.T. Perkins, D.E. Smith, S. Chu, Hydrodynamics of a DNA molecule in a flow field, Phys. Rev. E 55/2 (1997) 1794–1797.

[16] M.R.J. Verhoef, B.H.A.A. van den Brule, M.A. Hulsen, On the modelling of a PIB/PB Boger fluid in extensional flow. J. Non-Newtonian Fluid Mech., 1998, submitted for publication.

[17] G. Lielens, P. Halin, I. Jaumain, R. Keunings, V. Legat, New closure approximations for the kinetic theory of finitely extensible dumbbells, J. Non-Newtonian Fluid Mech. 76 (1998) 249–279.

[18] R. Sizaire, G. Lielens, I. Jaumain, R. Keunings, V. Legat, On the hysteretic behaviour of dilute polymer solutions in relaxation following extensional flow, J. Non-Newtonian Fluid Mech., May 1998, in press.

[19] P.S. Doyle, E.S.G. Shaqfeh, G.H. McKinley, S.H. Spiegelberg, Relaxation of dilute polymer solutions following extensional flow, J. Non-Newtonian Fluid Mech. 76 (1998) 79–110.

[20] H.C. Öttinger, Stochastic Processes in Polymeric Fluids: Tools and Examples for Developing Simulation Algorithms, Springer, Berlin, 1996.

[21] M. Herrchen, H.C. Öttinger, A detailed comparison of various FENE dumbbell models, J. Non-Newtonian Fluid Mech. 68 (1997) 17–42.

[22] R. Keunings, On the Peterlin approximation for finitely extensible dumbbells, J. Non-Newtonian Fluid Mech. 68 (1997) 85–100.

[23] A. Goublomme, B. Draily, M.J. Crochet, Numerical prediction of extrudate swell of a high-density polyethylene, J. Non-Newtonian Fluid Mech. 44 (1992) 171–195.

[24] H.C. Öttinger, B.H.A.A. van den Brule, M.A. Hulsen, Brownian configuration fields and variance reduced CONNFFESSIT, J. Non-Newtonian Fluid Mech. 70 (1997) 255–261.

[25] P. Halin, Ph.D. Thesis, Université catholique de Louvain, Belgium, in preparation.

[26] B. Purnode, M.J. Crochet, Flows of polymer solutions through contractions. Part 1. Flow of polyacrylamide solutions through planar contractions, J. Non-Newtonian Fluid Mech. 65 (1996) 269–289.

[27] P. Halin, R. Keunings, M. Laso, H.C. Öttinger, M. Picasso, Evaluation of a micro-macro computational technique in complex polymer flows, in: A. Ait-Kadi et al., (Eds.), Proc. 12th Int. Cong. on Rheology, 1996, pp. 401–402.

[28] W.J. ter Horst, Simulation of a viscoelastic flow in a journal bearing geometry using Brownian configuration fields. Technical Report, Msc internal report MEAH-172, Laboratory for Aero and Hydrodynamics, Delft University of Technology, January 1998.

[29] R. Aggarwal, R. Keunings, F.-X. Roux, Simulation of the flow of integral viscoelastic fluids on a distributed memory parallel computer, J. Rheol. 38(2) (1994) 405–419.

[30] P. Henriksen, R. Keunings, Parallel computation of the flow of integral viscoelastic fluids on a heterogeneous network of workstations, Int. J. Numer. Meth. Fluids 18 (1994) 1167–1183.

[31] R. Keunings, Parallel finite element algorithms applied to computational rheology, Computers Chem. Eng. 19(6/7) (1995) 64–669.

[32] K. Feigl, H.C. Öttinger, A new class of stochastic simulation models for polymer stress calculation, J. Chem. Phys. 109 (1998) 815–826.

[33] K. Feigl, H.C. Öttinger, Towards realistic rheological models for polymer melt processing, Macromol. Symp. 121 (1997) 187–203.